




Mitochondrial and Clearance Impairment in p.D620N VPS35 Patient-Derived Neurons

Zoé Hanss, PhD,¹  Simone B. Larsen, PhD,¹ Paul Antony, PhD,¹  Pauline Mencke, MSc,¹ François Massart, BSc,¹ Javier Jarazo, PhD,¹ Jens C. Schwamborn, PhD,¹  Peter A. Barbuti, PhD,^{1,2,3} George D. Mellick, PhD,⁴ and Rejko Krüger, MD^{1,3,5*}

¹Luxembourg Centre for Systems Biomedicine (LCSB), University of Luxembourg, Esch-sur-Alzette, Luxembourg

²Department of Pathology and Cell Biology, Columbia University Medical Center, New York, New York, USA

³Transversal Translational Medicine, Luxembourg Institute of Health (LIH), Strassen, Luxembourg

⁴Griffith Institute for Drug Discovery, Griffith University, Nathan, Australia

⁵Parkinson Research Clinic, Centre Hospitalier de Luxembourg (CHL), Luxembourg

ABSTRACT: Background: VPS35 is part of the retromer complex and is responsible for the trafficking and recycling of proteins implicated in autophagy and lysosomal degradation, but also takes part in the degradation of mitochondrial proteins via mitochondria-derived vesicles. The p.D620N mutation of VPS35 causes an autosomal-dominant form of Parkinson's disease (PD), clinically representing typical PD.

Objective: Most of the studies on p.D620N VPS35 were performed on human tumor cell lines, rodent models overexpressing mutant VPS35, or in patient-derived fibroblasts. Here, based on identified target proteins, we investigated the implication of mutant VPS35 in autophagy, lysosomal degradation, and mitochondrial function in induced pluripotent stem cell-derived neurons from a patient harboring the p.D620N mutation.

Methods: We reprogrammed fibroblasts from a PD patient carrying the p.D620N mutation in the VPS35 gene and from two healthy donors in induced pluripotent stem cells. These were subsequently differentiated into

neuronal precursor cells to finally generate midbrain dopaminergic neurons.

Results: We observed a decreased autophagic flux and lysosomal mass associated with an accumulation of α -synuclein in patient-derived neurons compared to controls. Moreover, patient-derived neurons presented a mitochondrial dysfunction with decreased membrane potential, impaired mitochondrial respiration, and increased production of reactive oxygen species associated with a defect in mitochondrial quality control via mitophagy.

Conclusion: We describe for the first time the impact of the p.D620N VPS35 mutation on autophago-lysosome pathway and mitochondrial function in stem cell-derived neurons from an affected p.D620N carrier and define neuronal phenotypes for future pharmacological interventions. © 2020 International Parkinson and Movement Disorder Society

Key Words: VPS35; induced pluripotent stem cells; mitochondrial impairment; Parkinson's disease; α -synuclein

***Correspondence to:** Dr. Rejko Krüger, LCSB, University of Luxembourg, Esch-sur-Alzette, 6 avenue du Swing, L-4367, Belvaux, Luxembourg; E-mail: rejko.krueger@uni.lu

Zoé Hanss and Simone B. Larsen contributed equally to this work.

Financial Disclosure/Conflict of Interest: RK has received research grants from Fonds National de Recherche de Luxembourg (FNR) as Coordinator of the National Centre for Excellence in Research on Parkinson's disease (NCER-PD), Coordinator of the Study on COVID-19 National survey for assessing Viral spread by Non-affected Carriers (CON-VINCE). RK received as well as speaker's honoraria and/or travel grants from Abbvie, Zambon and Medtronic and he participated as PI or site-PI for industry sponsored clinical trials without receiving honoraria.

Received: 6 March 2020; **Revised:** 2 October 2020; **Accepted:** 5 October 2020

Published online in Wiley Online Library
(wileyonlinelibrary.com). DOI: 10.1002/mds.28365

The functional characterization of Parkinson's disease (PD)-linked mutations has enabled the identification of impaired cellular pathways underlying the neurodegeneration of dopaminergic neurons of the substantia nigra.¹ Recently, based on a growing number of genes identified in monogenic forms of PD, alterations of endosomal trafficking came into focus as a pathway linked to the disease. The p.D620N mutation in VPS35 was identified by two independent research groups in 2011^{2, 3} and causes a rare autosomal-dominant form of PD, occurring in 1.3% of familial cases and 0.1% of all PD cases.⁴ The clinical phenotype of patients resembles the one of typical sporadic PD patients, although variability is present in terms of age of onset.^{3, 5} Furthermore,

VPS35 expression has been showed to be reduced in the substantia nigra of sporadic PD patients.⁶ Therefore, the study of the VPS35 pathway is of interest for a wide range of PD patients.

VPS35 is part of the retromer complex, responsible for the recycling of targeted transmembrane proteins from the early endosome back to the plasma membrane and the retrograde transport from the endosomal system towards the trans-Golgi network (TGN).⁷ The retromer is composed of VPS35, VPS29, VPS26A, or VPS26B, and various sorting nexins. The pathogenic p.D620N VPS35 does not intervene with the proper formation of the retromer.⁸

The retromer transports proteins essential to lysosomal clearance, carrying them to the TGN to avoid their degradation. One of the most studied cargo proteins of the retromer is the cation-independent mannose 6-phosphate receptor (CIMPR).⁹ CIMPR is an endosomal protein that transports procathepsin D from the endoplasmic reticulum (ER) to the lysosome and is essential for the maturation into the hydrolase cathepsin D. CIMPR is then recycled via the retromer. In cells with a deficiency in VPS35, either through knockdown or by expressing the p.D620N mutant protein, CIMPR is not properly recycled back to the TGN, which leads to the degradation of the receptor and the subsequent mistrafficking of cathepsin D.^{10–12} The retromer also recycles key autophagy proteins: Lamp2a, implicated in chaperone-mediated autophagy, and ATG9, a protein involved in the induction of autophagy. Retromer complexes containing mutant VPS35 can no longer bind their cargo proteins and, thus, these proteins cannot escape degradation by the lysosome.^{8, 13} Overall, the retromer is crucial for proper trafficking of lysosomal clearance proteins, and the p.D620N mutation in VPS35 was found to be associated with dysfunctional lysosomal clearance.¹²

Several studies have identified mitochondrial impairment in rodent dopaminergic neurons expressing p.D620N VPS35. It has been reported that p.D620N VPS35 directly interacts with Drp1 (dynamin-related protein 1), a key component in mitochondria fission, leading to fragmented mitochondria and cell death.¹⁴ Moreover, in dopaminergic neurons from mice depleted of VPS35 or expressing p.D620N VPS35, mitochondrial fragmentation was observed with reduced level of mitochondrial fusion protein Mfn2 (mitofusin 2).¹⁵ This was related to increased mitochondrial fragmentation, with decreased mitochondrial membrane potential (MMP) and impaired respiration.^{14, 15} Similar results were described in patient-derived fibroblasts.¹⁶ Overall, VPS35, by its central role in endosomal trafficking, regulates cellular and mitochondrial quality control.¹⁷

Most studies with VPS35 deficiency have been conducted in rodent dopaminergic neurons or VPS35

knockdown models. Similar loss of function phenotypes were observed in cell lines overexpressing p.D620N VPS35, or in patient-derived fibroblasts of p.D620N VPS35 carriers. To date there have been no studies investigating the effect of mutant p.D620N VPS35 on cellular phenotypes related to mitochondrial function, autophago-lysosomal pathway, and α -synuclein levels in patient-derived neuronal models. Here, we reprogrammed fibroblasts from one patient carrying the p.D620N VPS35 mutation and two gender-matched controls of similar age into induced pluripotent stem cells (iPSCs). Then, we differentiated iPSCs into small molecule neuronal precursor cells (smNPC) and further into neuronal populations enriched in dopaminergic neurons.¹⁸

We found that iPSC-derived neurons carrying the p.D620N mutation in VPS35 displayed severe mitochondrial dysfunction with decreased MMP, increased mitochondrial reactive oxygen species (ROS) level, and impaired respiration. Further, we found alterations in mitophagy and a decrease in overall autophagic flux that may be associated with the observed impaired lysosomal function. Moreover, these patient-derived neurons harboring the p.D620N VPS35 mutation displayed a typical accumulation of α -synuclein protein. This suggests that p.D620N VPS35 leads to a profound dysfunction of several cellular processes through its central role in trafficking of proteins.

Materials and Methods

Subjects

We included a male patient carrying the p.D620N mutation in VPS35, described previously by Follet et al¹⁰ and two healthy male controls from Tübingen Biobank Control 1 and Control 2. Skin biopsies were taken from each individual aged 73, 72, and 77 years, respectively.

Ethical approval for the generation and functional characterization of patient-derived iPSCs have been provided by informed consent.

Cell Culture and Treatments

For mitochondrial morphology, membrane potential, and ROS assessment, neurons were cultivated in neuronal medium without B27 and ascorbic acid (without antioxidants supplementation) 4 hours prior to the experiment. All treatments were performed in the neuronal medium without antioxidants. To assess the mitophagic clearance capacity, the edited neurons with the Rosella construct were treated with 10 μ M CCCP (carbonyl cyanide 3-chlorophenylhydrazone) (Abcam, Cambridge, UK) for 24 hours. For the autophagy experiment, neurons were treated with 100 nM Bafilomycin A1 (Enzo Life Sciences, Bruxelles, Belgium) for 24 hours.

For autophagy enhancement, neurons were treated with 25 or 50 nM rapamycin (Enzo Life Sciences) for 24 hours. All experiments were repeated on three to six independent neuronal differentiations.

Live Cell Imaging and Analysis

Mitochondria were visualized using 100 nM MitoTracker Green FM (Invitrogen, Gent, Belgium) in neuronal medium without antioxidants and lysosomes with 100 nM LysoTracker Deep Red (Invitrogen) in neuronal medium with or without antioxidants. At least five Z-stack images per well were acquired using a Zeiss spinning disk confocal microscope. All the raw image datasets used in this study are deposited online in our R3 lab of the University of Luxembourg (<https://webdav-r3lab.uni.lu/public/MitoNetworks/VPS35Neurons/>).

To segment mitochondria, the mitochondrial channel was pre-processed with a difference of Gaussians where the foreground image was convolved with a Gaussian of size 11 and standard deviation 1 and the subtracted background image with a Gaussian of size 11 and standard deviation 3 (Mito_DoG). Only pixels above threshold 3000 in Mito_DoG and an intensity above 5000 in the raw mitochondrial channel were considered as foreground pixels. The mitochondrial mask was defined by removing connected components with less than 10 pixels. Mitochondrial morphometrics were quantified as previously described.¹⁹ Additional data on mitochondrial network can be consulted in Zanin et al.²⁰

Mitorosella Sensor, Generation of the Lines, Image Acquisition and Analysis

The generation of the lines carrying the Rosella reporter was performed as previously described.²¹ Briefly, the tandem fluorescent proteins consisting of pH sensor fluorescent protein pHluorin (F64L, S65T, V193G, and H231Q) and DsRed were fused to the entire open reading frame of ATP5C1 serving as a mitochondrial targeting sequence, and placed in between the homology arms targeting the AAV1 safe harbour²² (Addgene plasmid #22075). A double-strand break for triggering homologous recombination was performed with the px330²³ (Addgene plasmid #42230) carrying the sgRNA targeting sequence for the safe harbor as described by Mali et al.²⁴ SmNPC from patients (VPS35 1_2) and control individuals (Control 1) were nucleofected (P3 Primary Cell 4D-Nucleofector, V4XP-3024; Lonza, Basel, Switzerland) with both constructs and expanded before purification by fluorescence-activated cell sorting (FACS) (Aria III; Beckton Dickinson, Franklin Lakes, NJ).

Images were obtained on an Opera QEHS confocal spinning disk microscope (Perkin Elmer, Waltham, MA) with a 60× water immersion objective (NA = 1.2).

pHluorin was excited with a 488 nm laser and detected on camera 1 behind a 520/35 bandpass filter, while DsRed was excited with a 561 nm laser and detected on camera 2 behind a 600/40 bandpass filter. A 568 dichroic mirror split the light towards the corresponding cameras. Both fluorescent channels were acquired simultaneously with a binning setting of 2. One plane and 15 fields per well were acquired. One pixel corresponds to 0.2152 μm . Differentiated neurons were maintained under normal incubation conditions (37°C, 5% CO₂, and 80% humidity) within the microscope in between and during the different acquisition time points.

The automated image analysis was performed through a series of pre-processing and thresholds in MATLAB (The MathWorks, Inc., Natick, MA) as previously described.²¹ Briefly, a difference of Gaussian of convoluted foreground and background images was used for detecting all the events in the field. For classifying the events either as a mitochondrial or mitophagic event, a combination of green to red fluorescence ratio analysis and morphological filtering based on difference of Gaussians thresholding was used. Those presenting a mean ratio value below 0.6 were classified as mitophagic events.

Flow Cytometry

Neurons were detached with Accutase (Sigma, Bornem, Belgium) and centrifuged at 300 g for 3 minutes. Batches of 200,000 cells were then incubated in the dye or in the buffer (unstained). MMP was assessed by staining the single-cell suspension with 200 nM tetramethylrhodamine ethyl ester (TMRE; Invitrogen) for 30 minutes at 37°C. To correct for mitochondrial mass, MitoTracker Green FM (Invitrogen) was used as a counterstaining. For mitochondrial ROS, the single-cell suspension was stained with 2 μM MitoSOX Red (Invitrogen) for 15 minutes at 37°C without CO₂. Cells were analyzed with the BD LSRFortessa flow cytometry analyser and the mean fluorescence intensity of each dye was assessed on at least 20,000 single cells by using FlowJo LLC software. Mean fluorescence of the unstained cells was subtracted to account for autofluorescence.

Oxygen Consumption Rate Measurement

Oxygen consumption rate (OCR) was measured in whole cells using the Seahorse XFe96 Cell Metabolism Analyser (Agilent, Diegem, Belgium). Neurons were plated in the Seahorse XFe96 well plates 24 hours prior to measuring at a density of 80,000 cells per well. The concentrations of mitochondrial toxins used were optimized for neurons according to the manufacturer's recommendations. The final concentrations of toxin used were: oligomycin (oligo) - 2 μM ; FCCP - 250 nM;

antimycin A (AA), and rotenone (rot) - 5 μ M. The cells of each well were lysed with radioimmuno-precipitation assay (RIPA) buffer after the experiment and the OCR of each well was corrected for protein amount. Statistics

Statistical analyses were performed with GraphPad Prism. The statistical analyses performed and the *P* value of each experiment can be found in the legend of the figures.

Data Availability

The authors confirm that the data supporting the findings of this study are available within the article and its supplementary material.

Results

Clinical Phenotype of p.D620N VPS35 Patient

The male patient donor case #2610 comes from a multi-incident family #445 reported previously from the Queensland Parkinson's Project,²⁵ that immigrated from Western Europe. Besides the index patient, the diagnosis of PD was made in his mother and maternal grandfather but no additional family members are known to be affected. The diagnosis of PD was made by a movement disorders neurologist after a 1-year history of muscular rigidity and tremor. The PD-related motor symptoms responded well to levodopa therapy. The index patient underwent deep brain stimulation 6 years after diagnosis after experiencing motor fluctuations with good treatment response.

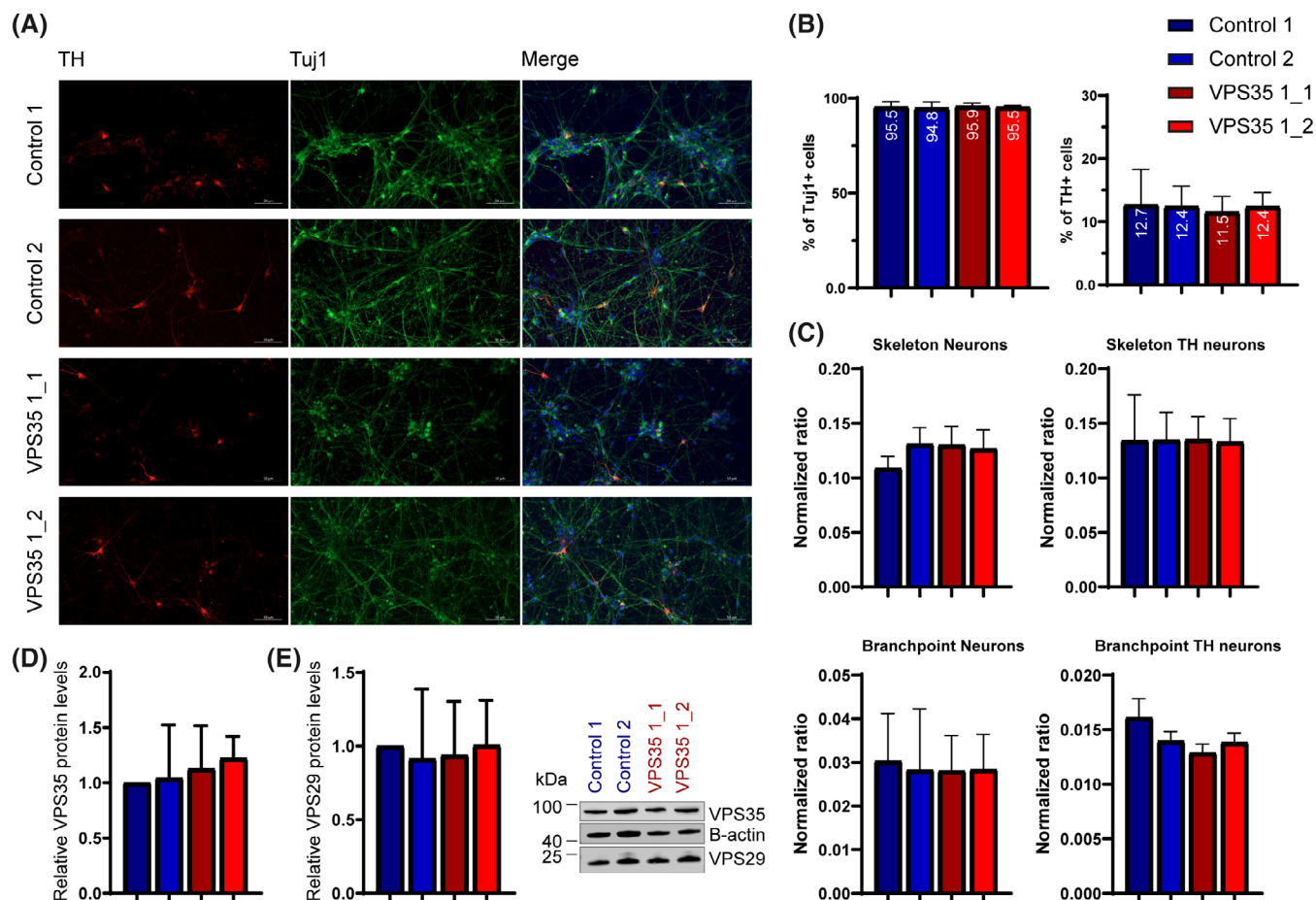


FIG. 1. No difference in neuronal morphology and network nor in levels of VPS35 and VPS29 proteins between patient and control induced pluripotent stem cell (IPSC)-derived neurons. **(A)** Representative images of immunofluorescence staining show expression of tyrosine hydroxylase (TH), class III β -tubulin (Tuj1), and nuclear DAPI in IPSC-derived neurons. **(B)** Fluorescence-activated cell sorting (FACS) analysis of neuronal culture revealed no difference in terms of percentage of dopaminergic neurons (TH+) among all neurons (Tuj1+) in control- and patient-derived neuronal cultures after 30 days of maturation (*n* = 4). **(C)** Analysis of the neuronal network by comparison of neurite length (skeleton) and number of branchpoints shows similar complexity between control- and patient-derived neurons. Values represent pixel count of skeleton or branchpoint normalized to the pixel count of the respective neuronal mask (*n* = 4). **(D,E)** Western blot analysis of VPS35 **(D)**, VPS29 **(E)**, and β -actin (loading control) show no difference in protein levels between control (Control 1 and 2) and VPS35 D620N mutant (VPS35 clones 1_1 and 1_2) neurons under basal culture condition. Values normalized to Control 1 (*n* = 4–6). [Color figure can be viewed at wileyonlinelibrary.com]

VPS35 and VPS29 Levels are Unchanged in p.D620N VPS35 Patient-Derived Neurons

Previous studies have reported that VPS35 protein levels did not change in cells carrying mutant VPS35.⁸ The p.D620N mutation in VPS35 has been shown not to impair its binding to the other components of the retromer.¹⁰ To investigate the levels of retromer components we differentiated iPSC from the index patient (VPS35 1_1 and 1_2)²⁶ and two age- and gender-matched controls (Control 1 and 2) into smNPC.¹⁸ All iPSC and smNPC clones were fully characterized in this study (Figs S1–S3) or elsewhere.²⁶ We successfully differentiated these smNPC into physiologically active neurons expressing the neuronal marker Tuj1 (tubulin β 3), enriched in dopaminergic neurons expressing tyrosine hydroxylase (TH) (Figs 1A and S4A–H).¹⁸ No difference was observed in terms of neuronal differentiation efficiency (Figs 1B and S4A, B) or neuronal network complexity between control- and patient-derived lines (Figs 1C and S4D). We identified by western blotting that protein levels of both retromer components VPS35 and VPS29 were unchanged between control- and patient-derived neurons (Fig. 1D,E).

P.D620N VPS35 Patient-Derived Neurons Display Mitochondrial Dysfunction

To evaluate the mitochondrial network, we analyzed Z-stack images from two controls and two clones of patient-derived neurons stained with MitoTracker Green FM (Fig. 2A). Computational analyses revealed a decrease in mitochondrial size representative of fragmentation (Fig. 2B). Moreover, mitochondrial branching as a readout for connectivity within the mitochondrial network was impaired with a decreased average number of links (Fig. 2C) and nodes (Fig. 2D).

The identification of these morphological alterations observed in patient-derived neurons led us to assess the mitochondrial function. We measured the bioenergetic profile and found a decreased MMP in patient-derived neurons compared to controls (Fig. 2E). The reduced MMP was accompanied by an increase of intra-mitochondrial ROS compared to controls (Fig. 2F). Subsequently, mitochondrial respiration was assessed by recording the OCR while we applied mitochondrial stressors: oligomycin, FCCP, antimycin A, and rotenone to measure different respiratory parameters (Fig. 2G). We found that neurons carrying the p.D620N VPS35 mutation displayed a reduced basal and maximal respiration, reduced spare respiratory capacity, and non-mitochondrial oxygen consumption (Fig. 2H). This was associated with a significantly reduced ATP production in patient-derived neurons compared to controls.

VPS35 D620N Patient-Derived Neurons Show an Impaired Mitochondrial Clearance

As patient neurons present morphologically and functionally altered mitochondria, we hypothesized that mitochondrial mass, biogenesis, and clearance (ie, mitophagy) might be dysregulated. We found no difference in mitochondrial mass between patient and control neurons as defined by western blotting against the mitochondrial proteins TOM20 (Fig. 3A) and VDAC1 (Fig. 3B). Moreover, protein expression levels of PGC1 α (Fig. 3C), the master regulator of mitochondrial biogenesis, were unchanged in patient-derived neurons under basal conditions.

In order to study mitophagy, Control 1 and VPS35 1_2 cell lines underwent CRISPR-Cas9 gene engineering as iPSC-derived smNPC to express a mitochondrial fusion protein: ATP5C1-DsRed-pHluorin. Briefly, when mitochondria are in the cytoplasm, both fluorophores are functional. Once mitochondria are exposed to an acidic environment inside the autophagosome (mitophagic event) the green fluorescence will be quenched (Fig. 3D). To induce mitophagic events, we treated the gene-edited neurons with CCCP and acquired images from the same field of view at different time points: $t = 0, 3, 8,$ and 24 hours. In control neurons (Fig. 3E), the number of mitochondria inside autophagosomes increased significantly after 3 hours CCCP treatment. After 8 hours and further after 24 hours of CCCP treatment, the number of mitochondria inside autophagosomes were decreasing, showing an efficient clearance. In the patient-derived neurons harbouring the p.D620N VPS35 (Fig. 3F), the number of mitochondria inside autophagosome also increased significantly after 3 hours of CCCP treatment. After 8 hours and 24 hours, the number of mitochondria inside autophagosomes failed to decrease and stayed elevated, indicating a deficient clearance (Fig. 3G). Under basal conditions ($t = 0$), we see no significant differences in the number of mitochondria inside autophagosomes between patient and control neurons. In addition, after 3 hours of CCCP treatment there was no difference in the number of mitochondria inside autophagosomes between patients and controls (Fig. 3G), indicating that the induction of mitophagy was not impaired in patient neurons. However, the difference between patient and control cells becomes significant at 8 hours and 24 hours, as the number of mitochondria inside autophagosomes decreased in control-derived neurons and stayed elevated in patient-derived neurons.

Lysosomal Clearance Dysfunction and α -Synuclein Accumulation in p.D620N VPS35 Patient-Derived Neurons

The link between the retromer and macroautophagy has been identified by the sorting of ATG9, an important protein for induction of autophagy with the

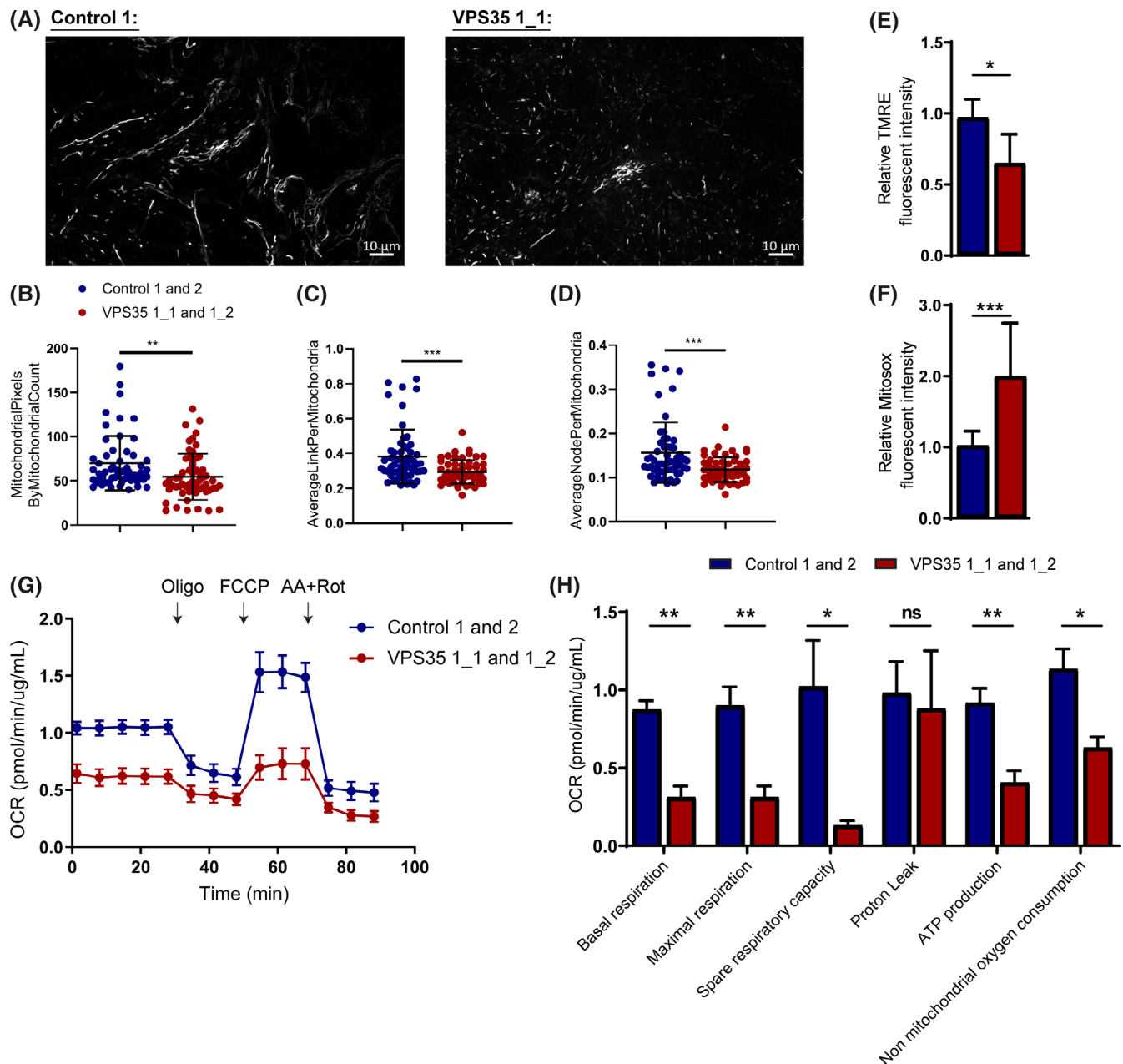


FIG. 2. Mitochondrial dysfunction in VPS35 mutant induced pluripotent stem cell (IPSC)-derived neurons. **(A)** Representative image of mitochondria stained with MitoTracker Green FM and evaluation of mitochondrial size **(B)**, average links per mitochondrion **(C)**, and average nodes per mitochondrion **(D)** in control (Control 1 and 2) and VPS35 D620N mutant (VPS35 clones 1_1 and 1_2) neurons in culture medium without antioxidants (without B27 and ascorbic acid) for 24 hours ($n = 4$). **(E)** Mitochondrial membrane potential measured by tetramethylrhodamine ethyl ester (TMRE) mean fluorescence intensity and **(F)** mitochondrial reactive oxygen species measured by MitoSOX mean fluorescence intensity by flow cytometry in control (Control 1 and 2) and VPS35 D620N mutant (VPS35 clones 1_1 and 1_2) neurons in culture medium without antioxidants (without B27 and ascorbic acid) for 4 hours ($n = 4$). **(G)** Mean average oxygen consumption rate (OCR) of control (Control 1 and 2) and VPS35 D620N mutant (VPS35 clones 1_1 and 1_2) neurons over a time course. Measurement of basal OCR is followed by the addition of oligomycin (oligo) 2 μM final concentration, FCCP 250 nM final concentration, and antimycin A (AA) 5 μM final concentration and rotenone (rot) 5 μM final concentration ($n = 4$). **(H)** Calculated basal respiration, maximal respiration, spare respiratory capacity, proton leak, ATP production, and non-mitochondrial oxygen consumption ($n = 4$). All statistical tests were Mann-Whitney tests to compare groups. Error bars show standard deviation and ns $P > 0.05$; * $P < 0.05$; ** $P < 0.01$; *** $P < 0.001$. [Color figure can be viewed at wileyonlinelibrary.com]

retromer.²⁷ Additionally, in cells overexpressing the mutant p.D620N VPS35 it was shown that ATG9 was missorted, which is thought to lead to impaired autophagy.⁸ Here, we measured the steady-state level of the autophagy protein p62 (Fig. 4A), which was not

differing between patient and control-derived neurons. Upon treatment with Bafilomycin A1, which blocks autophagy by inhibiting the lysosomal v-ATPase, p62 was accumulating in the controls, as shown by an increase compared to the untreated state. However,

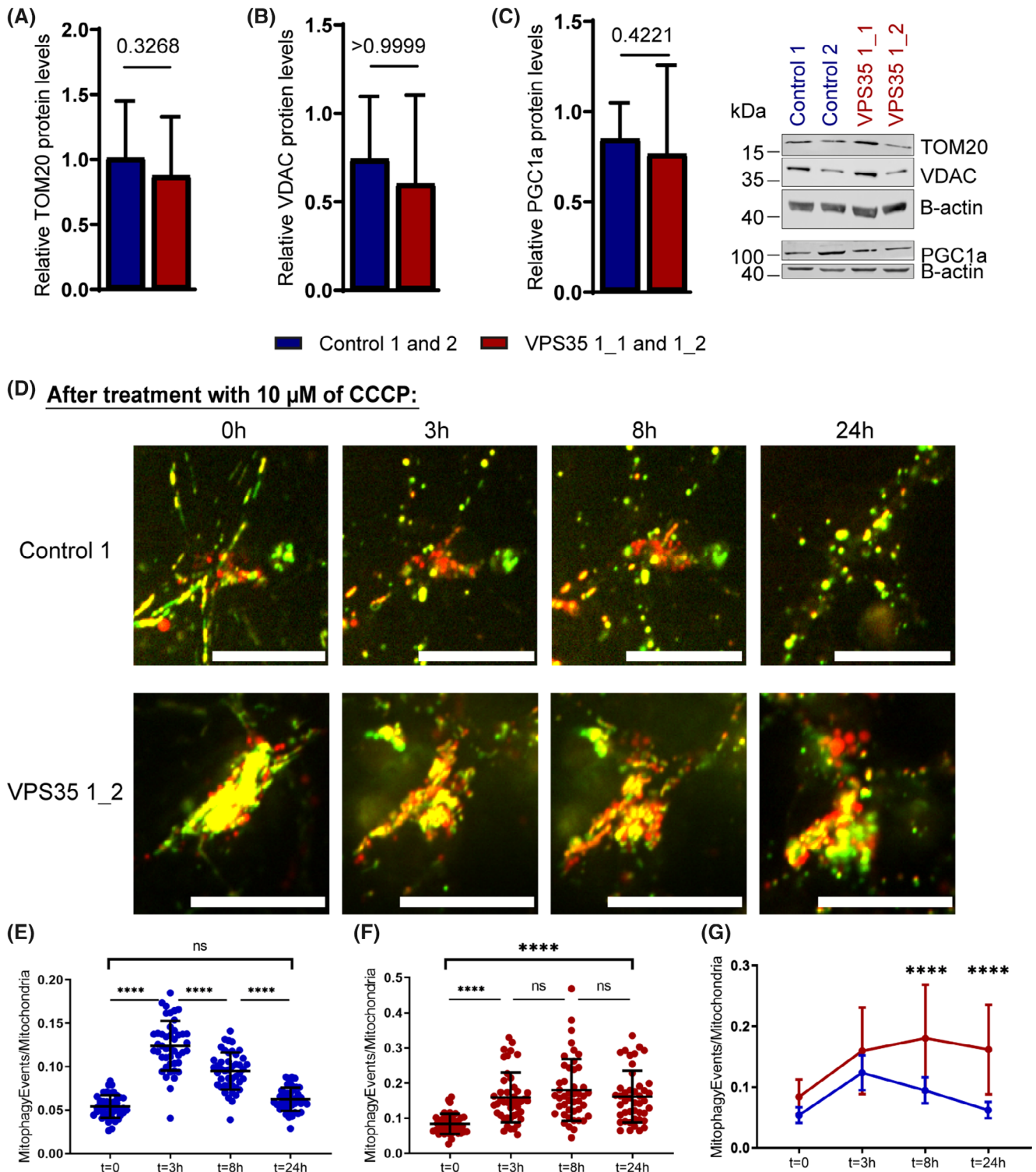


FIG. 3. Mitophagy clearance impairment in VPS35 mutant induced pluripotent stem cell (iPSC)-derived neurons after CCCP (carbonyl cyanide 3-chlorophenylhydrazone) treatment. **(A,B,C)** Western blot analysis of TOM20 **(A)**, VDAC **(B)**, PGC1 α **(C)**, and β -actin (loading control) of control (Control 1 and 2) and VPS35 D620N mutant (VPS35 clones 1_1 and 1_2) neurons under basal culture condition ($n = 4$). **(D)** Representative image of mitochondria and mitophagy events under CCCP treatment over a time course. The scale bar represents 20 μ m. Calculated mitophagic events by mitochondria count in Control 1 **(E)** and mutant VPS35 1_2 **(F)** from three independent differentiations of control (Control 1) and VPS35 D620N mutant (VPS35 clone 1_2) neurons expressing ATP5C1-RFP-pHluorin protein in culture medium without antioxidants (without B27 and ascorbic acid) and treated with CCCP 10 μ M for 0, 3, 8, and 24 hours. Each time point is compared with the previous one ($n = 3$). **(G)** Comparison of both lines. All statistical tests were Mann-Whitney tests or one-way ANOVA followed by Sidak's multiple comparisons tests to compare groups and conditions. Error bars show standard deviation and ns $P > 0.05$; * $P < 0.05$; ** $P < 0.01$; *** $P < 0.001$; **** $P < 0.0001$. [Color figure can be viewed at wileyonlinelibrary.com]

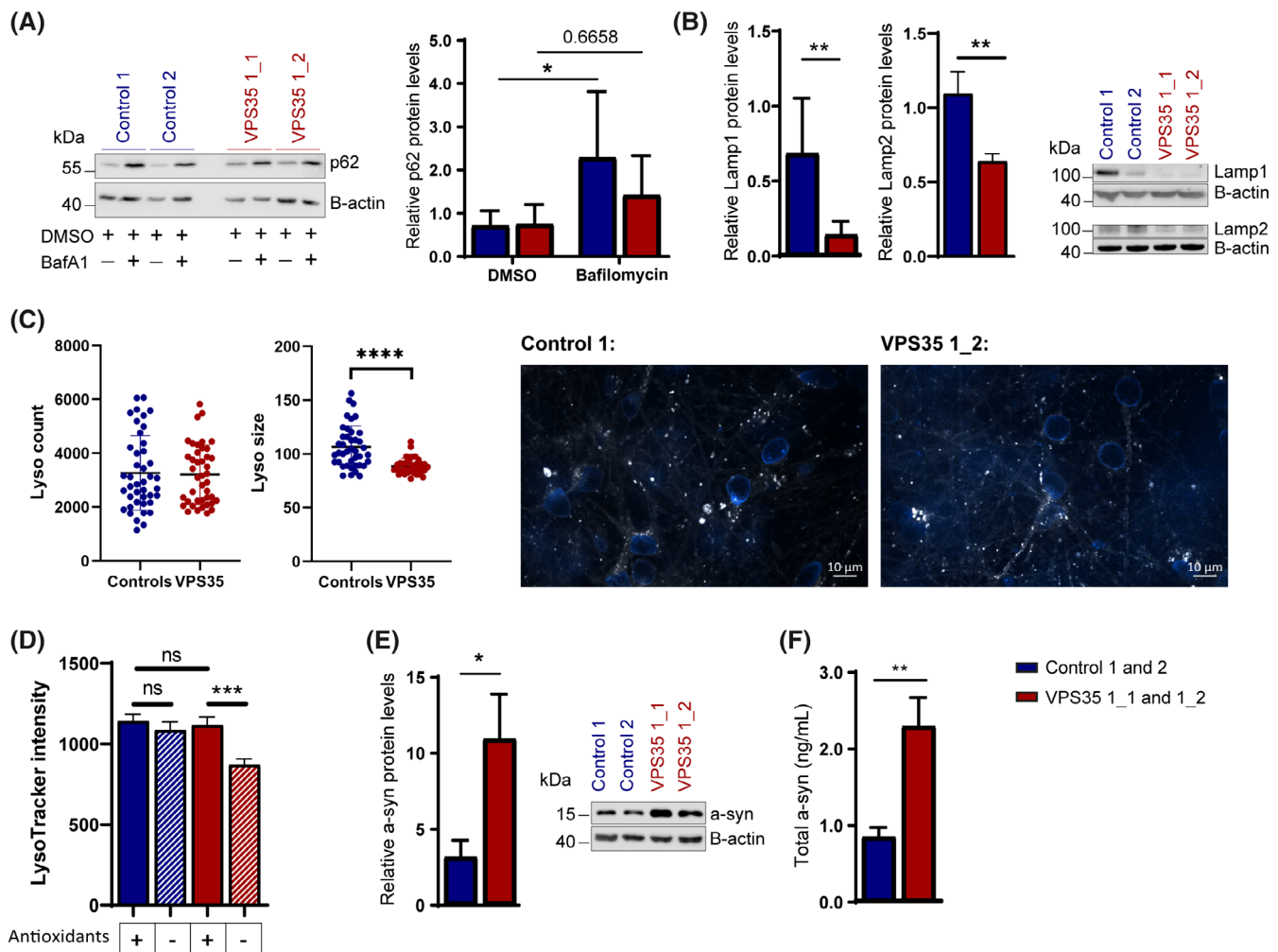


FIG. 4. Impaired lysosomal clearance and α -synuclein accumulation in VPS35 mutant induced pluripotent stem cell (IPSC)-derived neurons. **(A)** Western blot analysis of p62 and β -actin (loading control) in control (Control 1 and 2) and VPS35 D620N mutant (VPS35 clones 1_1 and 1_2) neurons under basal culture condition and Bafilomycin A1 (BafA1) 100 nM treatment for 24 hours ($n = 5$) **(B)** Western blot analysis of Lamp1, Lamp2, and β -actin (loading control) in control (Control 1 and 2) and VPS35 D620N mutant (VPS35 clones 1_1 and 1_2) neurons under basal culture condition ($n = 4$). **(C)** Left: evaluation of lysosomal size and number by LysoTracker staining in control (Control 1 and 2) and VPS35 D620N mutant (VPS35 clones 1_1 and 1_2) neurons under basal culture condition ($n = 3$). Right: representative images of lysosomes stained with LysoTracker Deep Red (white). Nucleus are stained with Hoechst. **(D)** Evaluation of LysoTracker Deep Red staining intensity in control (Control 1 and 2) and VPS35 D620N mutant (VPS35 clones 1_1 and 1_2) neurons under basal culture condition and mild stress (antioxidant removal) ($n = 3$). **(E)** Western blot analysis of α -synuclein (α -syn) and β -actin (loading control) in control (Control 1 and 2) and VPS35 D620N mutant (VPS35 clones 1_1 and 1_2) neurons under basal culture condition ($n = 4$) **(F)** Time-resolved fluorescence energy transfer (TR-FRET) measurement of total α -synuclein (α -syn) amount in control (Control 1 and 2) and VPS35 D620N mutant (VPS35 clones 1_1 and 1_2) neurons under basal culture condition ($n = 4$). All statistical tests were Mann-Whitney tests or one-way ANOVA followed by Sidak's multiple comparisons tests to compare groups and conditions. Error bars show standard deviation and * $P < 0.05$; ** $P < 0.01$; *** $P < 0.001$; **** $P < 0.0001$. [Color figure can be viewed at wileyonlinelibrary.com]

p62 did not significantly increase in the patient neurons after Bafilomycin A1 treatment, showing an impaired autophagic flux. Moreover, compared to control-derived neurons, we found reduced Lamp1 and Lamp2 steady-state protein levels in the patient neurons (Fig. 4B), suggesting a lower late-endosome/lysosome mass compared to controls. This decrease in Lamp1 and Lamp2 levels was accompanied by the presence of smaller lysosomes in patient-derived neurons, while the number of lysosomes was comparable between groups (Fig. 4C). This reduction in content and size of lysosome is implying an impaired functionality¹³ which is

also revealed by a decreased intensity of the acidotropic probe, LysoTracker, in patient-derived neurons when exposed to mild oxidative stress (antioxidant removal) (Fig. 4D) as already described in other genetic models of PD.²⁸

The impaired lysosomal clearance was accompanied by an increase of the amount of α -synuclein in patient-derived neurons as demonstrated by western blotting for the monomeric form of α -synuclein (Fig. 4E) and validated by time-resolved fluorescence energy transfer (TR-FRET) assessing total α -synuclein amount (Fig. 4F).

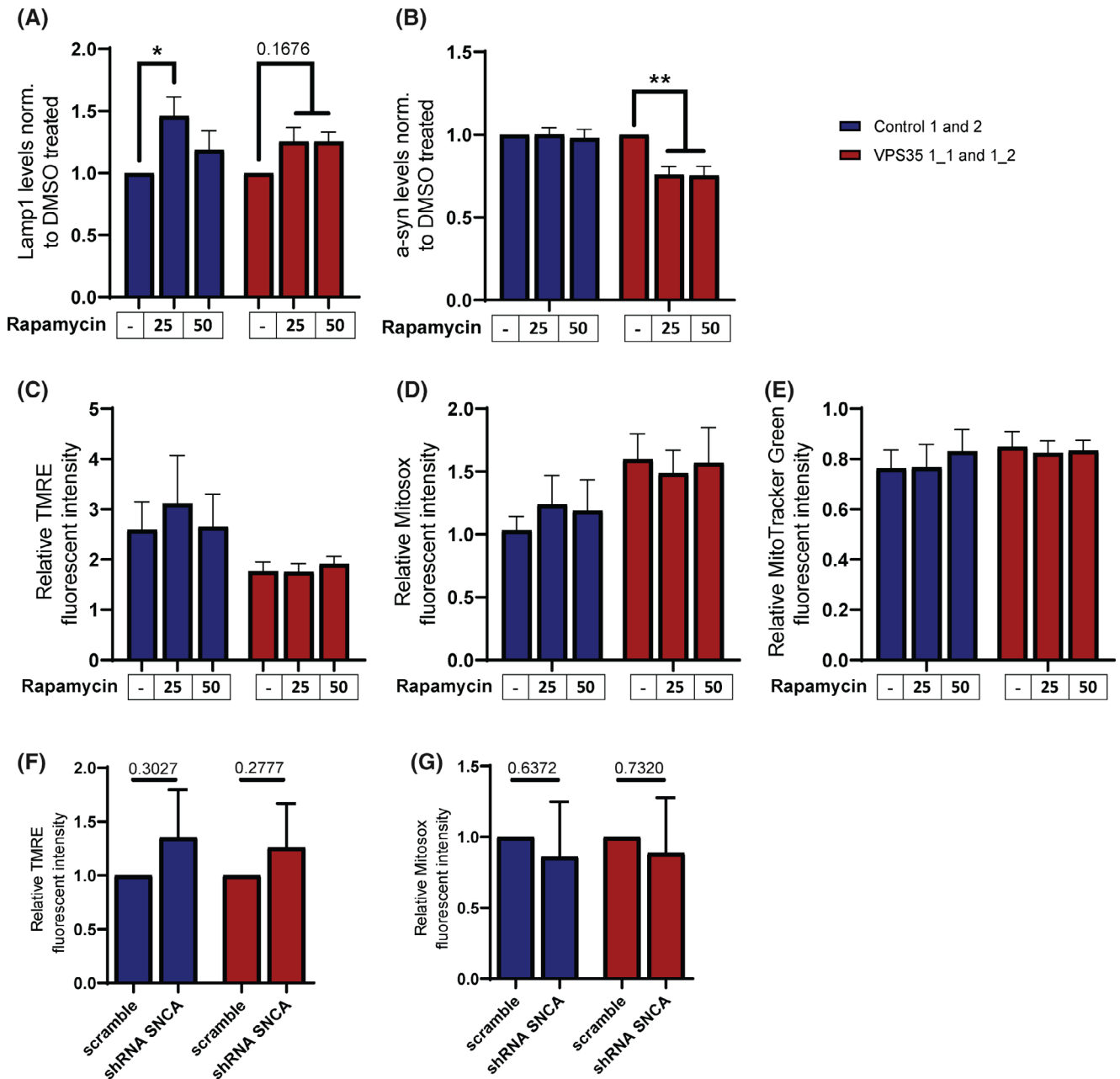


FIG. 5. Autophagy enhancement and α -synuclein knockdown are not sufficient to alleviate mitochondrial dysfunction. **(A,B)** Western blot analysis of Lamp1 **(A)** and α -synuclein **(B)** of control and VPS35 D620N mutant neurons after 24 hours of treatment with DMSO (50 nM) or rapamycin (25 or 50 nM) ($n = 5$). Values are normalized to DMSO-treated line respectively. **(C)** Mitochondrial membrane potential measured by tetramethylrhodamine ethyl ester (TMRE) mean fluorescence intensity, **(D)** mitochondrial reactive oxygen species measured by MitoSOX mean fluorescence intensity, and **(E)** mitochondrial mass measured by MitoTracker Green FM mean fluorescence intensity by flow cytometry in control and VPS35 D620N mutant neurons after 24 hours of treatment with DMSO (50 nM) or rapamycin (25 or 50 nM) ($n = 5$). Values are normalized to DMSO-treated Control 1. **(F)** Mitochondrial membrane potential measured by TMRE mean fluorescence intensity and **(G)** mitochondrial reactive oxygen species measured by MitoSOX mean fluorescence intensity by flow cytometry in control and VPS35 D620N mutant neurons transduced with scramble shRNA and shRNA against α -synuclein ($n = 3$). Values are normalized to scramble transduced line respectively. All statistical tests were Mann-Whitney tests or one-way ANOVA followed by Sidak's multiple comparisons tests to compare groups and conditions. Error bars show standard deviation and * $P < 0.05$; ** $P < 0.01$. [Color figure can be viewed at wileyonlinelibrary.com]

α -Synuclein Accumulation is not the Main Cause of Mitochondrial Impairment in pD620N VPS35 Neurons

In patient-derived neurons carrying a triplication of the SNCA gene locus, extensive mitochondrial defects

are found.^{29, 30} Consequently, we hypothesized that the mitochondrial impairment seen in our patient-derived neurons could be due to both a general impairment of the autophagy machinery and to α -synuclein accumulation. Therefore, we used a pharmacological approach

to rescue autophagy with rapamycin.³¹ Rapamycin has been shown to increase lysosomal biogenesis and to enhance mitophagy in cellular models of PD.^{32, 33} After 24 hours of treatment, Lamp1 levels were increased in both control- and patient-derived neurons (Fig. 5A) and this led to a moderate decrease of α -synuclein levels in patient-derived neurons (Fig. 5B). We evaluated the effect of this treatment on mitochondrial dysfunction but did not observe a rescue of the decreased MMP nor of the increased ROS levels in patient-derived lines (Fig. 5C,D). Of note, mitochondrial mass was not affected (Fig. 5E), which shows that rapamycin did not enhance basal mitophagy in these experimental conditions. We hypothesized that a more efficient decrease of α -synuclein levels might influence the mitochondrial impairment. We knocked-down α -synuclein in both control- and patient-derived neurons with shRNA against *SNCA*.³⁴ After transduction, we detected a reduction of the levels of α -synuclein in patient-derived neurons to the physiological levels of α -synuclein (Fig. S5A,B). Using the same technique as previously, we found that the reduction of α -synuclein protein levels did not rescue the loss of MMP (Fig. 5F) nor the increased ROS level (Fig. 5G).

Discussion

The increasing importance of endosomal trafficking pathways in PD pathogenesis has been widely recognized besides established pathways such as mitochondrial impairment, lysosomal dysfunction, protein aggregation, and synaptic dysfunction.³⁵ Indeed, numerous *PARK* genes (*DNAJC13*, *LRRK2*, and *SNCA*) are implicated in this pathway and there is a growing interest in finding other disease-relevant endosomal trafficking genes.³⁶

VPS35 deficiency has been previously linked to mitochondrial and lysosomal clearance impairment in multiple cellular models such as dopaminergic neurons from mice carrying a heterozygous loss of VPS35, rat cortical neurons overexpressing p.D620N VPS35, and patient fibroblasts carrying the p.D620N VPS35 mutation. These studies consistently report fragmented mitochondria with decreased MMP and impaired respiration.^{14–16} Moreover, decreased autophagic flux together with impaired cathepsin D and Lamp2a trafficking was also previously described in other models.⁵ In this study, we demonstrate for the first time in patient-specific iPSC-derived neurons that the PD-causing mutation p.D620N in VPS35 leads to fragmented and impaired mitochondria with decreased size and branching, decreased membrane potential, increased mitochondrial ROS, and dysfunctional respiration (Fig. 2). These defects were linked to dysfunctional mitochondrial clearance with accumulation of mitophagic

events under mitochondrial stress without completion of the full mitophagic process (Fig. 3). Lysosomal clearance was also more globally impaired with decreased autophagic flux, decreased late-endosome/lysosome mass and size, and impaired acidification (Fig. 4A–D). Possibly linked to the lysosomal dysfunction, we observed an accumulation of α -synuclein in patient-derived neurons (Fig. 4E,F).

We hypothesize that mitochondrial impairment in iPSC-derived neurons carrying the p.D620N VPS35 mutation is caused by a substantially impaired mitochondrial quality control linked to a more general autophagy defect. Improving autophagic function by rapamycin treatment reduced α -synuclein levels in patient-derived neurons, showing the involvement of lysosomal dysfunction in α -synuclein accumulation, but the mitochondrial dysfunction remained (Fig. 5A–D). As it is known that the induction of autophagy via rapamycin is only mild in mammalian cells, for example, compared to yeast cells,³⁷ we used a more stringent reduction of α -synuclein levels via RNA knockdown. However, also this was not sufficient to significantly improve mitochondrial function (Fig. 5F,G) and shows that α -synuclein accumulation is not the main cause of mitochondrial impairment in p.D620N VPS35 neurons.

Further pharmacological and genetic modification of the lysosome, as well as alternative organellar degradation pathways, may help to better understand the link between lysosomal dysfunction and mitochondrial impairment. Indeed, previous studies also reported that VPS35 and the retromer are involved in an alternative subtype of mitochondrial quality control, via the formation of mitochondria-derived vesicles (MDVs).³⁸ Two cargos have been identified trafficking towards the lysosome or the peroxisome for degradation, namely Drp1¹⁴ and MAPL (mitochondrial-associated protein ligase).^{15, 38} MAPL is known to stabilize Drp1, a mitochondrial fission protein, and degrade Mfn2, a mitochondrial fusion protein. By trafficking both proteins, VPS35 seems to stabilize the mitochondrial network in a fused state. In cells overexpressing p.D620N VPS35, the retromer does not correctly transport Drp1 and MAPL, which leads to increased MAPL and Drp1 protein levels and a decreased Mfn2 protein level. This subsequently leads to a fragmented mitochondrial network,^{14, 15} also observed in patient-derived neurons in our study. Interestingly, treatment of cells overexpressing p.D620N VPS35 and patient fibroblasts carrying the p.D620N VPS35 variant with Mdivi1, a Drp1 inhibitor, rescues the mitochondrial functional impairment.^{14, 16} This suggests that mitochondrial functional impairment is at least in part caused by the mistrafficking of Drp1 and MAPL by the retromer-containing mutant p.D620N VPS35.

Although providing evidence for novel cellular phenotypes related to mutant VPS35 in patient-derived

neurons, our study has limitations towards the specificity of these findings for the dopaminergic pathway. In order to directly assess a specific role of mutations of VPS35 on dopaminergic neurons, single-cell analyses of these neurons within a mixed culture including glial cells or a cell-sorting of dopaminergic neurons for enrichment prior to experiments would allow evaluation of the specific contribution of these observed cellular phenotypes for dopaminergic neurons. Previous findings on iPSC-derived neurons with heterozygous VPS35 mutations³⁹ suggested that the p.D620N VPS35 mutation acts by a loss-of-function mechanism, while animal models using overexpression of human mutant VPS35 tend to support a toxic gain-of-function or a dominant-negative mechanism.^{40, 41} The present data show conserved levels of VPS35 protein and suggest an impairment of physiological functions of VPS35. The next steps to better qualify the p.D620N mutation would include the investigation of the described phenotypes on a larger panel of patient-derived VPS35 D620N lines as well as overexpression of the wild-type and mutant protein in different cell types. Also, the inclusion of isogenic controls would allow dissection of the specific contribution of the p.D620N VPS35 mutation within the individual genetic background of the controls and the patient, which may influence the disease phenotype by itself. Taken together, our findings provide the first evidence for mitochondrial impairment, lysosomal degradation defects, and α -synuclein accumulation in patient-derived neurons, which confirm the implication of the p.D620N VPS35 mutation in the typical pathophysiology of PD. ■

Acknowledgments: Patient fibroblasts were obtained from Griffith University. We would like to thank Prof. Peter Silburn for clinical updates on this patient. Control fibroblasts were obtained from the Neuro-Biobank of the University of Tuebingen, Germany (<https://www.hih-tuebingen.de/en/about-us/core-facilities/biobank/>). This biobank is supported by the local University, the Hertie Institute, and the DZNE. We thank Christine Bus from the University of Tuebingen for the plasmids and protocol for reprogramming. pX330-U6-Chimeric_BB-CBh-hSpCas9 was a gift from Feng Zhang (Addgene plasmid # 42230). AAVS1 SA-2A-puro-pA donor was a gift from Rudolf Jaenisch (Addgene plasmid # 22075). We would like to thank Prof. T. Graham and A. Sargsyan from the University of Utah for kindly providing us with the pHluorin construct.

References

1. Krüger R, Klucken J, Weiss D, Tönges L, Kolber P, Unterecker S, et al. Classification of advanced stages of Parkinson's disease: translation into stratified treatments. *J Neural Trans* 2017;124(8):1015–1027.
2. Vilariño-Güell C, Wider C, Ross OA, Dachsel JC, Kachergus JM, Lincoln SJ, et al. VPS35 mutations in Parkinson disease. *Am J Hum Genet* 2011;89(1):162–167. <https://www.unfpa.org/sites/default/files/pub-pdf/De-linkingFGMfromIslamfinalreport.pdf>. Accessed February 17 2020.
3. Zimprich A, Benet-Pagès A, Struhal W, Graf E, Eck SH, Offman MN, et al. A mutation in VPS35, encoding a subunit of the retromer complex, causes late-onset Parkinson disease. *Am J Hum Genet*. 2011;89(1):168–175. <http://www.ncbi.nlm.nih.gov/pubmed/21763483>. Accessed February 17, 2020.
4. Deng H, Gao K, Jankovic J. The VPS35 gene and Parkinson's disease. *Mov Disord* 2013;28(5):569–575. <http://www.ncbi.nlm.nih.gov/pubmed/23536430>. Accessed February 17, 2020.
5. Mohan M, Mellick GD. Role of the VPS35 D620N mutation in Parkinson's disease. *Parkinsonism Relat Disord* 2017;36:10–18. <http://www.ncbi.nlm.nih.gov/pubmed/27964832>. Accessed February 17, 2020.
6. MacLeod DA, Rhinn H, Kuwahara T, Zolin A, Di Paolo G, McCabe BD, et al. RAB7L1 interacts with LRRK2 to modify intraneuronal protein sorting and Parkinson's disease risk. *Neuron* 2013;77(3):425–439. <https://linkinghub.elsevier.com/retrieve/pii/S0896627312011208>. Accessed June 12, 2020.
7. Seaman MN, McCaffery JM, Emr SD. A membrane coat complex essential for endosome-to-Golgi retrograde transport in yeast. *J Cell Biol* 1998;142(3):665–681. <http://www.ncbi.nlm.nih.gov/pubmed/9700157>. Accessed February 17, 2020.
8. Zavodszky E, Seaman MNJ, Moreau K, Jimenez-Sanchez M, Breusegem SY, Harbour ME, et al. Mutation in VPS35 associated with Parkinson's disease impairs WASH complex association and inhibits autophagy. *Nat Commun* 2014;5:3828. <http://www.ncbi.nlm.nih.gov/pubmed/24819384>. Accessed February 17, 2020.
9. Arighi CN, Harmell LM, Aguilar RC, Haft CR, Bonifacio JS. Role of the mammalian retromer in sorting of the cation-independent mannose 6-phosphate receptor. *J Cell Biol* 2004;165(1):123–133.
10. Follett J, Norwood SJ, Hamilton NA, Mohan M, Kovtun O, Tay S, et al. The Vps35 D620N mutation linked to Parkinson's disease disrupts the cargo sorting function of retromer. *Traffic* 2014;15(2):230–244. <http://www.ncbi.nlm.nih.gov/pubmed/24152121>. Accessed February 17, 2020.
11. McGough IJ, Steinberg F, Jia D, Barbuti PA, McMillan KJ, Heesom KJ, et al. Retromer binding to FAM21 and the WASH complex is perturbed by the Parkinson disease-linked VPS35(D620N) mutation. *Curr Biol* 2014;24(14):1670–1676. <http://www.ncbi.nlm.nih.gov/pubmed/24980502>. Accessed February 17, 2020.
12. Miura E, Hasegawa T, Konno M, Suzuki M, Sugeno N, Fujikake N, et al. VPS35 dysfunction impairs lysosomal degradation of α -synuclein and exacerbates neurotoxicity in a drosophila model of Parkinson's disease. *Neurobiol Dis* 2014;71:1–13.
13. Tang F-L, Erion JR, Tian Y, Liu W, Yin D-M, Ye J, et al. VPS35 in dopamine neurons is required for endosome-to-golgi retrieval of Lamp2a, a receptor of chaperone-mediated autophagy that is critical for α -synuclein degradation and prevention of pathogenesis of Parkinson's disease. *J Neurosci* 2015;35(29):10613–10628.
14. Wang W, Wang X, Fujioka H, Hoppel C, Whone AL, Caldwell MA, et al. Parkinson's disease-associated mutant VPS35 causes mitochondrial dysfunction by recycling DLP1 complexes. *Nat Med* 2016;22(1):54–63.
15. Tang FL, Liu W, Hu JX, Erion JR, Ye J, Mei L, et al. VPS35 deficiency or mutation causes dopaminergic neuronal loss by impairing mitochondrial fusion and function. *Cell Rep* 2015;12(10):1631–1643.
16. Zhou L, Wang W, Hoppel C, Liu J, Zhu X. Parkinson's disease-associated pathogenic VPS35 mutation causes complex I deficits. *Biochim Biophys Acta Mol Basis Dis* 2017;1863(11):2791–2795. <http://www.ncbi.nlm.nih.gov/pubmed/28765075>. Accessed February 17, 2020.
17. Larsen SB, Hanss Z, Krüger R. The genetic architecture of mitochondrial dysfunction in Parkinson's disease. *Cell Tissue Res* 2018;373(1):21–37. <http://www.ncbi.nlm.nih.gov/pubmed/29372317>. Accessed June 13, 2019.
18. Reinhardt P, Glatza M, Hemmer K, Tsytsyura Y, Thiel CS, Höing S, et al. Derivation and expansion using only small molecules of human neural progenitors for neurodegenerative disease modeling. *PLoS One* 2013;8(3):e59252. <http://www.ncbi.nlm.nih.gov/pubmed/23533608>. Accessed February 17, 2020.
19. Baumratov AS, Antony PMA, Ostaszewski M, He F, Salamanca L, Antunes L, et al. Enteric neurons from Parkinson's disease patients display ex vivo aberrations in mitochondrial structure. *Sci Rep* 2016;6:33117. <http://www.ncbi.nlm.nih.gov/pubmed/27624977>. Accessed February 17, 2020.

20. Zanin M, Santos BFR, Antony PMA, Berenguer-Escuder C, Larsen SB, Hanss Z, et al. Mitochondria-mitochondria interaction networks show altered topological patterns in Parkinson's disease. *bioRxiv* 2020;984195. <https://doi.org/10.1038/s41540-020-00156-4>. Accessed March 10, 2020.
21. Arias-Fuenzalida J, Jarazo J, Walter J, Gomez-Giro G, Forster JJ, Krueger R, et al. Automated high-throughput high-content autophagy and mitophagy analysis platform. *Sci Rep* 2019;9(1): 9455. <http://www.ncbi.nlm.nih.gov/pubmed/31263238>. Accessed February 17, 2020.
22. Hockemeyer D, Soldner F, Beard C, Gao Q, Mitalipova M, DeKelver RC, et al. Efficient targeting of expressed and silent genes in human ESCs and iPSCs using zinc-finger nucleases. *Nat Biotechnol* 2009;27(9):851–857.
23. Cong L, Ran FA, Cox D, Lin S, Barretto R, Habib N, et al. Multiplex genome engineering using CRISPR/Cas systems. *Science* 2013; 339(6121):819–823. <http://www.ncbi.nlm.nih.gov/pubmed/23287718>. Accessed July 9, 2019.
24. Mali P, Yang L, Esvelt KM, Aach J, Guell M, DiCarlo JE, et al. RNA-guided human genome engineering via Cas9. *Science* 2013; 339(6121):823–826.
25. Bentley SR, Bortnick S, Guella I, Fowdar JY, Silburn PA, Wood SA, et al. Pipeline to gene discovery—analysing familial parkinsonism in the Queensland Parkinson's project. *Park Relat Disord* 2018;49: 34–41. <http://www.ncbi.nlm.nih.gov/pubmed/29329938>. Accessed February 17, 2020.
26. Larsen SB, Hanss Z, Cruciani G, Massart F, Barbuti PA, Mellick G, et al. Induced pluripotent stem cell line (LCSBi001-a) derived from a patient with Parkinson's disease carrying the p.D620N mutation in VPS35. *Stem Cell Res* 2020;45:101776. <https://doi.org/10.1016/j.scr.2020.101776>
27. Popovic D, Dikic I. TBC1D5 and the AP2 complex regulate ATG9 trafficking and initiation of autophagy. *EMBO Rep* 2014;15(4): 392–401. <http://www.ncbi.nlm.nih.gov/pubmed/24603492>. Accessed February 17, 2020.
28. Kriebel G, Ruckerbauer S, Burbulla LF, Kieper N, Maurer B, Waak J, et al. Reduced basal autophagy and impaired mitochondrial dynamics due to loss of Parkinson's disease-associated protein DJ-1. Petrucelli L, editor. *PLoS One* 2010;5(2):e9367. <http://www.ncbi.nlm.nih.gov/pubmed/20186336>. Accessed February 23, 2010.
29. Zambon F, Cherubini M, Fernandes HJR, Lang C, Ryan BJ, Volpato V, et al. Cellular α -synuclein pathology is associated with bioenergetic dysfunction in Parkinson's iPSC-derived dopamine neurons. *Hum Mol Genet* 2019;28(12):2001–2013. <http://www.ncbi.nlm.nih.gov/pubmed/30753527>. Accessed August 2, 2019.
30. Little D, Luft C, Mosaku O, Lorvellec M, Yao Z, Paillusson S, et al. A single cell high content assay detects mitochondrial dysfunction in iPSC-derived neurons with mutations in SNCA. *Sci Rep* 2018;8(1): 9033. <https://pubmed.ncbi.nlm.nih.gov/29899557/>. Accessed July 23, 2020.
31. Sarkar S, Ravikumar B, Floto RA, Rubinsztein DC. Rapamycin and mTOR-independent autophagy inducers ameliorate toxicity of polyglutamine-expanded huntingtin and related proteinopathies. *Cell Death Differ* 2009;16:46–56. <https://pubmed.ncbi.nlm.nih.gov/18636076/>. Accessed July 23, 2020.
32. Dehay B, Bové J, Rodríguez-Muela N, Perier C, Recasens A, Boya P, et al. Pathogenic lysosomal depletion in Parkinson's disease. *J Neurosci* 2010;30(37):12535–12544.
33. Burbulla LF, Fitzgerald JC, Stegen K, Westermeier J, Thost A-K, Kato H, et al. Mitochondrial proteolytic stress induced by loss of mortalin function is rescued by Parkin and PINK1. *Cell Death Dis* 2014;5(4):e1180. <http://www.nature.com/doi/10.1038/cddis.2014.103>.
34. Mazzulli JR, Zinke F, Isacson O, Studer L, Krainc D. α -Synuclein-induced lysosomal dysfunction occurs through disruptions in protein trafficking in human midbrain synucleinopathy models. *Proc Natl Acad Sci USA* 2016;113(7):1931–1936.
35. Perrett RM, Alexopoulou Z, Tofaris GK. The endosomal pathway in Parkinson's disease. *Mol Cell Neurosci* 2015;66 (Pt A):21–28. <http://www.ncbi.nlm.nih.gov/pubmed/25701813>. Accessed February 17, 2020.
36. Bandres-Ciga S, Saez-Atienzar S, Bonet-Ponce L, Billingsley K, Vitale D, Blauwendraat C, et al. The endocytic membrane trafficking pathway plays a major role in the risk of Parkinson's disease. *Mov Disord* 2019;34(4):460–468.
37. Thoreen CC, Sabatini DM. Rapamycin inhibits mTORC1, but not completely. *Autophagy*. Taylor and Francis Inc. 2009;5:725–726. <https://pubmed.ncbi.nlm.nih.gov/19395872/>. Accessed July 31, 2020.
38. Braschi E, Zunino R, HM MB. MAPL is a new mitochondrial SUMO E3 ligase that regulates mitochondrial fission. *EMBO Rep* 2009;10(7): 748–754. <http://www.ncbi.nlm.nih.gov/pubmed/19407830>. Accessed February 17, 2020.
39. Munsie LN, Milnerwood AJ, Seibler P, Beccano-Kelly DA, Tatarnikov I, Khinda J, et al. Retromer-dependent neurotransmitter receptor trafficking to synapses is altered by the Parkinson's disease VPS35 mutation p.D620N. *Hum Mol Genet* 2015;24(6):1691–1703.
40. Tsika E, Glauser L, Moser R, Fiser A, Daniel G, Sheerin UM, et al. Parkinson's disease-linked mutations in VPS35 induce dopaminergic neurodegeneration. *Hum Mol Genet* 2014;23(17): 4621–4638.
41. Chen X, Kordich JK, Williams ET, Levine N, Cole-Strauss A, Marshall L, et al. Parkinson's disease-linked D620N VPS35 knockin mice manifest tau neuropathology and dopaminergic neurodegeneration. *Proc Natl Acad Sci USA* 2019;116(12):5765–5774.

Supporting Data

Additional Supporting Information may be found in the online version of this article at the publisher's web-site.

SGML and CITI Use Only DO NOT PRINT

Authors' Contributions

Z.H., S.B.L., P.A.B., and R.K. designed the experiments. S.B.L., Z.H., P.M., F.M., and P.A.B. performed the cell culture and performed the experiments. P.A. wrote the script and analyzed the neuronal and mitochondrial network. J.J. and J.C.S. generated the CRISPR-modified lines and performed the mitophagy experiments and analysis. G.D.M. obtained the patients' fibroblasts. Z.H. and S.B.L. drafted the manuscript with input from R.K. and P.A.B. All authors reviewed the manuscript and agreed on the final version.

Financial Disclosures

This study was supported by grants from the Fond National de Recherche within the PEARL programme (FNR/P13/6682797 to R.K.), the NCER-PD programme (NCER13/BM/11264123), and by the European Union's Horizon2020 research and innovation programme under grant agreement No. 692320 (WIDESPREAD; CENTRE-PD). This project was also supported by the European Union's Horizon 2020 research and innovation programme under grant agreement No. 668738, SysMedPD. J.J. is supported by a Pelican award from the Fondation du Pelican de Mie et Pierre Hippert-Faber.